3d conservative coupling method between a compressible fluid flow and a deformable structure

Maria Adela Puscas[*†‡], Virginie Daru[‡], Alexandre Ern[*], Christian Mariotti[†], Laurent Monasse[*], Christian Tenaud[‡]

[*] Université Paris-Est, CERMICS, École des Ponts ParisTech
77455 Marne la Vallée cedex, France
email: {puscasa, ern, monassel}@cermics.enpc.fr

[†] CEA, DAM, DIF, F-91297 Arpajon, France
email: {adela.puscas, christian.mariotti}@cea.fr

[‡] LIMSI-CNRS, 91403 Orsay, France
email: {adela.puscas, virginie.daru, christian.tenaud}@limsi.fr

ABSTRACT

In this work, we present a conservative method for three-dimensional inviscid fluid-structure interaction problems. On the fluid side, we consider an inviscid Euler fluid in conservative form. The Finite Volume method uses the OSMP high-order flux with a Strang operator directional splitting [1]. On the solid side, we consider an elastic deformable solid. In order to examine the issue of energy conservation, the behavior law is here assumed to be linear elasticity. In order to ultimately deal with rupture, we use a Discrete Element method for the discretization of the solid [2]. An immersed boundary technique is employed through the modification of the Finite Volume fluxes in the vicinity of the solid. Since both fluid and solid methods are explicit, the coupling scheme is designed to be globally explicit too. The computational cost of the fluid and solid methods lies mainly in the evaluation of fluxes on the fluid side and of forces and torques on the solid side. The coupling algorithm evaluates these only once every time step, ensuring the computational efficiency of the coupling. Our approach is an extension to the three-dimensional deformable case of the conservative method developed in [3]. We focus herein numerical results assessing the robustness of the method in the case of a undeformable solid with large displacements subjected to a compressible fluid flow.

1 Introduction

Many situations involve phenomena of fluid-structure interactions. The study of such phenomena is motivated by the fact that the consequences are sometimes catastrophic for the mechanical structure. For example, in the military or safety domains, the effects of an explosion on a building or on a submarine involve complex non-linear phenomena (shock waves, cracking, rupture, ...) [12]. In view of these applications, we consider on the fluid side an inviscid compressible fluid flow model so as to deal with air shock waves and on the solid side an elastic deformable solid.

The main challenges in fluid-structure interaction problems are the computation of the fluid forces that act on the rigid or deformable structure and the modification of the fluid domain due to the displacement of the solid. Another difficulty that arises in fluid-structure interaction problems is the coupling of models with different descriptions: the fluid is classically described in Eulerian formulation and the elastic structure in Lagrangian formulation. Several types of methods have been developed for this purpose. Fully Eulerian [10], fully Lagrangian [11], Arbitrary Lagrangian-Eulerian (ALE) methods [4] and fictitious domain methods ([5], [7], [8]) have been proposed to address the issue of fluid-structure interaction. In general, monolithic Eulerian or Lagrangian approaches are limited to the case where the fluid and solid behave according to similar equations with different parameters. The ALE method deforms the fluid domain in order to follow the movement of the structure. It is a method with adapted mesh on the solid boundaries which requires possibly costly re-meshing of the fluid domain when the solid goes through large displacement or rupture.

In fictitious domain methods the solid is superimposed on the fluid fixed grid, and additional terms are introduced in the fluid formulation to penalize or prevent the penetration of fluid inside the solid. Various

types of fictitious domain methods have been developed: Immersed Boundary methods [5], Ghost Fluid methods [6], Embedded Boundary methods [7], etc.
An important issue in compressible fluid-structure interaction is the conservation of mass, momentum and energy. The accurate capture of shocks is based on conservation properties and the preservation of physical properties is an important ingredient towards an effective numerical method. In addition, verifying conservation at a discrete level is a natural means to prove the numerical stability of the scheme. Embedded Boundary methods [8] are built in such a way that the spatial discretization satisfies mass, momentum and energy conservation.
We therefore use the Embedded Boundary method developed by Colella *et al.* [8] in combination with a Finite Volume method for the fluid and a Discrete Element method for the solid. The Finite Volume method is computed on a Cartesian grid, using high-order upwind fluxes [1] computed with a Lax-Wendroff approach. The Discrete Element method [2] is a particle method for elastodynamics, in which particles interact through forces and torques yielding the macroscopic behaviour of the assembly. Both methods being time-explicit and computationally expensive, we require that the coupling algorithm be explicit too. The method is tailored to yield the exact conservation of mass, momentum and energy of the system and exhibits consistency properties. A conservative explicit coupling algorithm between the Finite Volume method and 2d undeformable solid has already been developed in [3]. Herein we extend the results to the 3d deformable case.
This paper starts with a brief description of the fluid and solid methods. Then, we present the proposed conservative coupling method and the explicit time-integration coupling procedure between the inviscid fluid and the deformable moving structure. Next, we point out several properties of the coupling method. Finally, we present numerical results showing the energy and mass conservation by the coupling scheme and the ability of the method to compute the interaction of strong discontinuities with irregular moving boundaries.

2 Fluid and solid description

2.1 Inviscid compressible flow

The fluid is modeled by the Euler equations expressing conservation of mass, momentum and energy for an inviscid compressible flow, which are written in Cartesian coordinates:

$$\frac{\partial U}{\partial t} + \frac{\partial F(U)}{\partial x} + \frac{\partial G(U)}{\partial y} + \frac{\partial H(U)}{\partial z} = 0, \tag{1}$$

$$U = \begin{pmatrix} \rho \\ \rho u \\ \rho v \\ \rho w \\ \rho E \end{pmatrix}, F(U) = \begin{pmatrix} \rho u \\ \rho u^2 + p \\ \rho uv \\ \rho uw \\ (\rho E + p)u \end{pmatrix}, G(U) = \begin{pmatrix} \rho v \\ \rho uv \\ \rho v^2 + p \\ \rho vw \\ (\rho E + p)v \end{pmatrix}, H(U) = \begin{pmatrix} \rho w \\ \rho uw \\ \rho vw \\ \rho w^2 + p \\ (\rho E + p)w \end{pmatrix},$$

where ρ is the mass density, p the pressure, (u, v, w) the velocity vector and E the total energy. The pressure in the fluid is modeled by the state equation of a perfect gas: $p = (\gamma - 1)\rho e$, e being the specific internal energy with $E = e + \frac{1}{2}(u^2 + v^2 + w^2)$ and $\gamma = 1.4$ the ratio of specific heats, assumed to be constant.
The numerical resolution of these equations is based on a Cartesian grid explicit Finite Volume method and directional operator splitting. For the flux calculation we use the OSMP numerical scheme which is a one-step high order scheme [1]. It is derived using a coupled space-time Lax-Wendroff approach, where the formal order of accuracy in the scalar case can be set at an arbitrary order. In this work we use order 11. The coupling method is actually independent from the numerical scheme used for the flux calculation.

2.2 Deformable solid discretization method

The deformable solid is modeled using a Discrete Element method. The solid is discretized with a finite number of rigid particles. Each particle is governed by the classical equations of mechanics and interparticle links ensure the macroscopic behaviour of the solid [2]. The solid is discretized into polyhedral

particles which have a rigid-body motion and interact through forces and torques. The expression of these forces and torques allows one to recover the macroscopic behaviour of materials. Furthermore, this approach facilitates the handling of rupture and fracture, because breaking the link between material grains ensures the loss of cohesion between solid particles.
The position and velocity of the solid particles are given respectively by the position of their center of mass $\mathbf{X}$, the rotation matrix $\mathbf{Q}$, the velocity of the center of mass $\mathbf{V}$ and the angular momentum matrix $\mathbf{P}$. The movement of solid particles is integrated in time by an explicit scheme using the Verlet scheme for translation and the RATTLE scheme for rotation [3].

3 Coupling method

Fluid-structure interaction needs to take into account the solid obstacles in the flow calculation as well as the fluid efforts on the solid. For the first point we use a method of immersed boundaries which allows for easy modification of existing fluid solvers. In this context, the solid and fluid grid overlap, leading to fluid-solid mixed cells, thereafter called "cut-cells".

3.1 Cut-cells description

Since the solid is discretized into polyhedral particles, the fluid-solid interface is simply the set of faces of these polyhedra in contact with the fluid.
We denote with integer subscripts i, j, k quantities related to the center of cells and with half integer subscripts quantities related to the center of faces. Let $C_{i,j,k}$ be a cut-cell of size $(\Delta x_{i,j,k},\ \Delta y_{i,j,k},\ \Delta z_{i,j,k})$ and $\Omega_S(t)$ the solid domain. The relevant aspects of the intersection between the moving interface and cell $C_{i,j,k}$ are:

- the **volume fraction** $0 \leqslant \Lambda_{i,j,k} \leqslant 1$ occupied by the solid in the cell $C_{i,j,k}$:

$$\Lambda_{i,j,k}(t) = \frac{\mathcal{V}_{i,j,k}(t)}{V_{i,j,k}}, \tag{2}$$

  $V_{i,j,k} = (\Delta x\, \Delta y\, \Delta z)_{i,j,k}$ being the volume of $C_{i,j,k}$ where the solid occupies the volume $\mathcal{V}_{i,j,k}(t)$ at instant t:

$$\mathcal{V}_{i,j,k}(t) = \int_{C_{i,j,k} \cap \Omega_S(t)} dx\, dy\, dz.$$

  The volume fraction is evaluated at the discrete time t^n. The interface between cells $C_{i,j,k}$ and $C_{i+1,j,k}$ is denoted $\partial C_{i+1/2,j,k}$.

- the **side area fraction** $0 \leqslant \lambda_{i\pm1/2,j,k}, \lambda_{i,j\pm1/2,k}, \lambda_{i,j,k\pm1/2} \leqslant 1$ of each face; for example on face $\partial C_{i+1/2,j,k}$ we have

$$\lambda^{n+1/2}_{i+1/2,j,k} = \frac{\mathcal{A}^{n+1/2}_{i+1/2,j,k}}{(\Delta y \Delta z)_{i,j,k}}, \tag{3}$$

  where $\mathcal{A}^{n+1/2}_{i+1/2,j,k}$ is the area representing the intersection of the solid with face $\partial C_{i+1/2,j,k}$ averaged over $\left[t^n, t^{n+1}\right]$:

$$\mathcal{A}^{n+1/2}_{i+1/2,j,k} = \frac{1}{\Delta t} \int_{t^n}^{t^{n+1}} \int_{\partial C_{i+1/2,j,k} \cap \Omega_S(t)} dy\, dz\, dt.$$

- the **boundary area** denoted $A^{n+1/2}_{f_{i,j,k}}$, is the area of the surface formed by the intersection of the fluid with the solid in the cell during the time interval $\left[t^n, t^{n+1}\right]$:

$$A^{n+1/2}_{f_{i,j,k}} = \frac{1}{\Delta t} \int_{t^n}^{t^{n+1}} \int_{C_{i,j,k} \cap \partial\, \Omega_S(t)} ds\, dt.$$

  We also denote $\vec{n}_{f_{i,j,k}}(t)$ **the outward normal** to the surface (see Fig. 1).

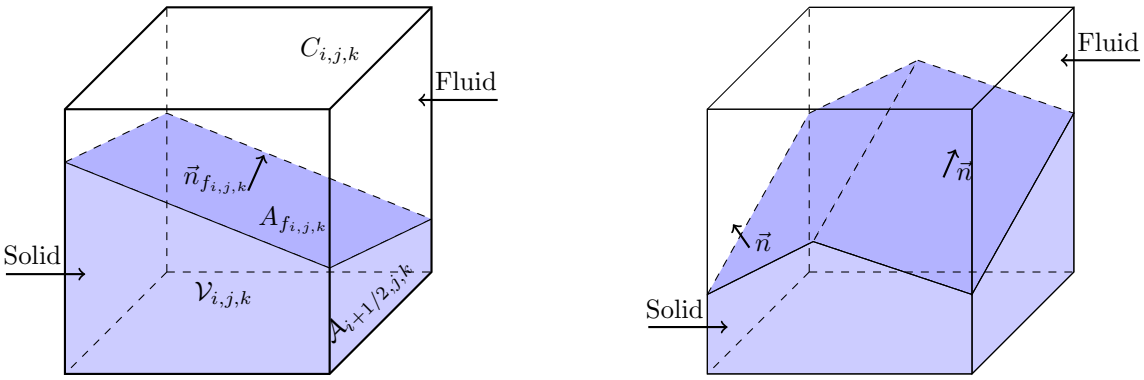

Figure 1: Description of a cut-cell

3.2 Treatment of the cut-cells

To take into account the position of the solid in the fluid domain, we rely on the immersed boundary method which modifies the fluid fluxes in cut-cells.
Consider a fluid cell partially intersected by a solid, as shown in Fig. 1. Integrating (1) on this cut-cell and over the time interval $[n\Delta t, (n+1)\Delta t]$ and applying the divergence theorem, yields

$$\begin{aligned}\left(1-\Lambda_{i,j,k}^{n+1}\right)U_{i,j,k}^{n+1} = \left(1-\Lambda_{i,j,k}^{n}\right)U_{i,j,k}^{n} + \Delta t \left\{ \frac{(1-\lambda_{i-1/2,j,k}^{n+1/2})}{\Delta x_{i,j,k}} F_{i-1/2,j,k} - \frac{(1-\lambda_{i+1/2,j,k}^{n+1/2})}{\Delta x_{i,j,k}} F_{i+1/2,j,k} \right. \\ + \frac{(1-\lambda_{i,j-1/2,k}^{n+1/2})}{\Delta y_{i,j,k}} G_{i,j-1/2,k} - \frac{(1-\lambda_{i,j+1/2,k}^{n+1/2})}{\Delta y_{i,j,k}} G_{i,j+1/2,k} \\ \left. + \frac{(1-\lambda_{i,j,k-1/2}^{n+1/2})}{\Delta z_{i,j,k}} H_{i,j,k-1/2} - \frac{(1-\lambda_{i,j,k+1/2}^{n+1/2})}{\Delta z_{i,j,k}} H_{i,j,k+1/2} \right\} \\ + \sum_{f\in C_{i,j,k}} A_{f_{i,j,k}}^{n+1/2}\,\phi_{f_{i,j,k}}^{n+1/2}.\end{aligned} \tag{4}$$

The additional flux ϕ_f results from the presence of the solid boundaries f in the cell $C_{i,j,k}$. This flux takes into account the exchange of energy and momentum between the solid and the fluid results from pressure forces.
The computation of average time of the side area fraction $\lambda^{n+1/2}$ and of the boundary area $A_f^{n+1/2}$ can be very complex and 3d implementation would be highly time consuming [7]. Instead, we take λ^{n+1} and A_f^{n+1}, and we calculate directly the conservative state given by the discrete balance in the cell, as in [3]:

$$\begin{aligned}\left(1-\Lambda_{i,j,k}^{n+1}\right)U_{i,j,k}^{n+1} = \left(1-\Lambda_{i,j,k}^{n+1}\right)U_{i,j,k}^{n} + \Delta t \left\{ \frac{(1-\lambda_{i-1/2,j,k}^{n+1})}{\Delta x_{i,j,k}} F_{i-1/2,j,k} - \frac{(1-\lambda_{i+1/2,j,k}^{n+1})}{\Delta x_{i,j,k}} F_{i+1/2,j,k} \right. \\ + \frac{(1-\lambda_{i,j-1/2,k}^{n+1})}{\Delta y_{i,j,k}} G_{i,j-1/2,k} - \frac{(1-\lambda_{i,j+1/2,k}^{n+1})}{\Delta y_{i,j,k}} G_{i,j+1/2,k} \\ \left. + \frac{(1-\lambda_{i,j,k-1/2}^{n+1})}{\Delta z_{i,j,k}} H_{i,j,k-1/2} - \frac{(1-\lambda_{i,j,k+1/2}^{n+1})}{\Delta z_{i,j,k}} H_{i,j,k+1/2} \right\} \\ + \frac{\Delta t}{V_{i,j,k}} \sum_{f\in C_{i,j,k}} A_{f_{i,j,k}}^{n+1}\phi_{f_{i,j,k}}^{n+1} + \sum_{f\in C_{i,j,k}} \Delta U_{f_{i,j,k}}^{n,n+1}.\end{aligned} \tag{5}$$

The term $\Delta U_{f_{i,j,k}}^{n,n+1}$ denotes the amount of U^n swept by the movement of the interface f during the time step; the amount swept by the movement of the interface f is such that

$$\sum_{C_{i,j,k}} \sum_{f \in C_{i,j,k}} \Delta U^{n,n+1}_{f_{i,j,k}} = \sum_{C_{i,j,k}} (\Lambda^{n+1}_{i,j,k} - \Lambda^{n}_{i,j,k}) U^{n}_{i,j,k}.$$

In practice, we decompose the interface into triangles which are contained in one cell (not necessarily the same) at times $n\Delta t$ and $(n+1)\Delta t$. We calculate $\Delta U^{n,n+1}_{f_{i,j,k}}$ as the integral of U^n on the prism built on these triangular bases. The detailed procedure to obtain these terms will be given in [13].
The main limitation of immersed boundary methods is that they involve small control cells ("small" in the sense that the solid volume fraction is > 0.5). In order to ensure the CFL stability condition of explicit schemes on these cells, the time step should be decreased to an unacceptably small value.
To deal with these issues, we use a conservative mixing process following the ideas developed in [9] with minor changes. Let p be a small cell and g a completely fluid $(\Lambda_g = 0)$ neighboring cell. We define the following exchange terms:

$$E_{pg} = \frac{(1-\Lambda_g)}{(2-\Lambda_p-\Lambda_g)}(U_g - U_p), \quad E_{gp} = \frac{(1-\Lambda_p)}{(2-\Lambda_p-\Lambda_g)}(U_p - U_g),$$

and we set

$$U_p = U_p + E_{pg}, \quad U_g = U_g + E_{gp}. \tag{6}$$

The mixing procedure is fully conservative and ensures that the equivalent volume of a mixed cell is compatible with the usual CFL condition using the standard size cells.

3.3 Coupling algorithm with a deformable solid

At the beginning of the time step $t^{n+1} = (n+1)\Delta t$, we known the state of the fluid $U^n_{i,j,k}$, the position and rotation of the particle $(\mathbf{X}^n, \mathbf{Q}^n)$, as well as the velocity of the center of mass and the angular momentum $(\mathbf{V}^n, \mathbf{P}^n)$. The general procedure for the conservative coupling method can be described by the following five steps:

1. The fluid fluxes are precomputed. We denote by $\overline{p}_x$, $\overline{p}_y$ and $\overline{p}_z$ the mean pressures used to compute the fluxes in the x, y and z directions.

2. The fluid forces $\vec{F}_f$ acting on a planar solid boundary f of surface A_f and normal vector $\vec{n}_f$ are equal to the force exerted by these pressures on the surface in contact with the fluid:

$$\vec{F}_f \cdot \vec{e}_x = -\overline{p}_x A_f n^x_f, \tag{7}$$
$$\vec{F}_f \cdot \vec{e}_y = -\overline{p}_y A_f \; n^y_f, \tag{8}$$
$$\vec{F}_f \cdot \vec{e}_z = -\overline{p}_z A_f n^z_f. \tag{9}$$

3. The solid is advanced in time: internal forces are computed based on the position of the solid particles. The position of each particle (submitted to a constant external fluid force) is integrated using the Verlet scheme for translation and the RATTLE scheme for rotation [3].

4. The volume fractions of solid in fluid cells $\Lambda^{n+1}_{i,j,k}$ and surface fractions of solid on cell interfaces $\lambda^{n+1}_{i\pm1/2,j,k}, \lambda^{n+1}_{i,j\pm1/2,k}, \lambda^{n+1}_{i,j,k\pm1/2}$ can then be computed using the new position of the solid boundary. The fluid fluxes are modified using $\Lambda^{n+1}_{i,j,k}$, $\Lambda^{n}_{i,j,k}$, $\lambda^{n+1}_{i\pm1/2,j,k}, \lambda^{n+1}_{i,j\pm1/2,k}, \lambda^{n+1}_{i,j,k\pm1/2}$, pressures $\overline{p}_x, \overline{p}_y$ and $\overline{p}_z$ and the velocity of the boundary in order to enforce the conservation of fluid mass and of the total momentum and energy of the system.

5. The final value of the state $U^{n+1}_{i,j,k}$ in the cell is calculated using (5). Owing to the perfect slip conditions at the solid boundary, the flux $\phi^{n+1}_{f_{i,j,k}}$ is given by

$$\phi^{n+1}_{f_{i,j,k}} = \frac{1}{A^{n+1}_{f_{i,j,k}}} \left(0,\, \Pi_x,\, \Pi_y,\, \Pi_z,\, \mathbf{V}^{n+1/2}_f \cdot \Pi\right)^t, \tag{10}$$

where

$$\Pi = \left(\int_f \bar{p}_x^{n+1} \, n_{f_{i,j,k}}^{n+1,\,x}, \int_f \bar{p}_y^{n+1} \, n_{f_{i,j,k}}^{n+1,\,y}, \int_f \bar{p}_z^{n+1} \, n_{f_{i,j,k}}^{n+1,\,z} \right)^t,$$

and $\mathbf{V}_f^{n+1/2}$ is the velocity in the center of the interface in the cell $C_{i,j,k}$:

$$\mathbf{V}_f^{n+1/2} = V^{n+1/2} + \Omega^{n+1/2} \wedge (X_f^{n+1} - X^{n+1}),$$

where X_f^{n+1} is the center of the part of interface f at time $(n+1)\Delta t$ in the cell, X^{n+1} the center of the particle containing f, and $V^{n+1/2}$ and $\Omega^{n+1/2}$, respectively, the average velocity and rotation velocity of the particle in the time interval $[n\Delta t,\, (n+1)\Delta t]$.

The general structure of the explicit coupling scheme is presented in Fig. 2.

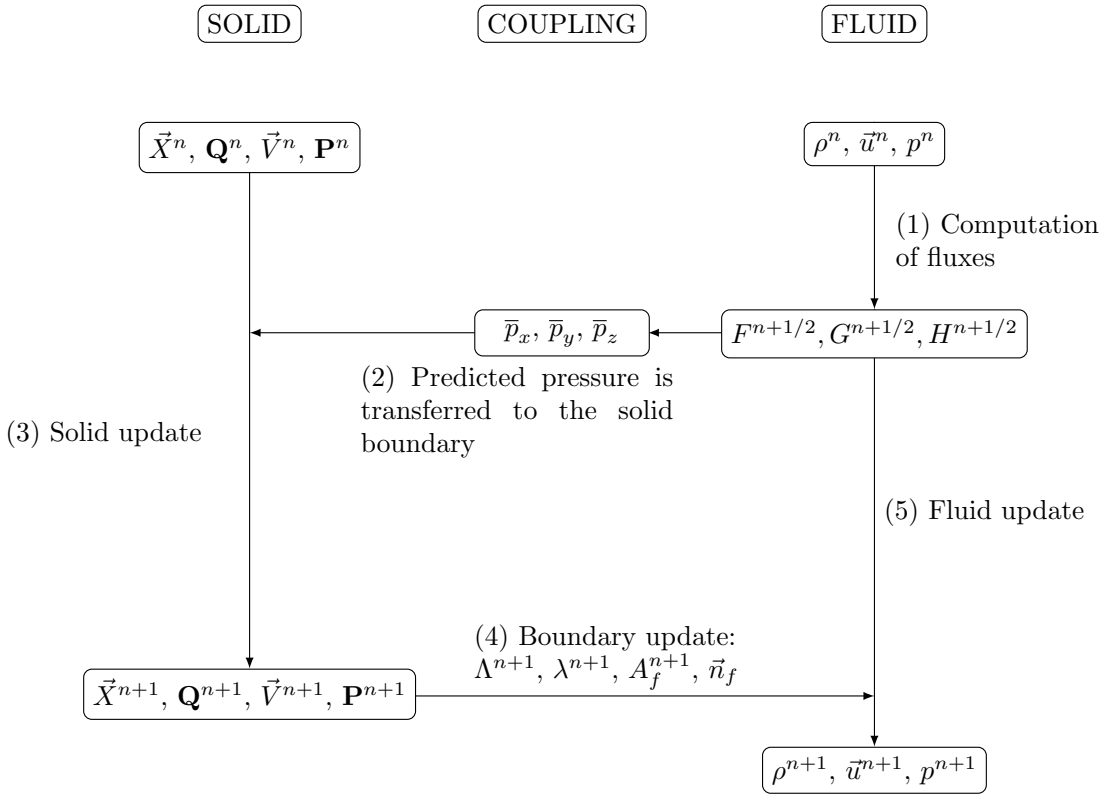

Figure 2: Structure of the explicit coupling scheme

3.4 Properties of the coupling scheme

The properties stated in this section can be proven and we have verified them numerically (see [3] for the proof in 2d; the proof in 3d is similar).

Conservation of mass, momentum and energy

These properties hold for periodic boundary conditions and in the cases where there is physical conservation (i.e. mass and energy with fixed boundaries, conservation when boundaries are far ...).

Perfect slipping along a wall

The coupling algorithm preserves exactly a uniform constant flow parallel to a rigid half-plane, even in the case when the solid is not aligned with the fluid grid. This last result shows that no artificial roughness appears on the solid walls.

Galilean invariance

Consider an arbitrary shaped rigid body moving at constant velocity and without rotation, immersed in a uniform fluid flowing at the same velocity. Then, the uniform movement of the fluid and the solid is retained by the coupling algorithm.

4 Numerical results

4.1 Conservation of mass and energy

In order to verify the conservation by the coupling scheme, we consider a test consisting in a simple shock tube in a straight rectangular channel and a rigid mobile body inside this channel. The computational domain is a simple rectangular box $(x, y, z) \in [0, 2] \times [0, 1] \times [0, 1]$ and the initial flow field is given by

$$\begin{cases} \rho = 1.4,\ u = v = w = 0,\ p = 5 & \text{if } x < 0.16, \\ \rho = 1.4,\ u = v = w = 0,\ p = 1, & \text{if } x \geq 0.16. \end{cases} \tag{11}$$

The solid is represented by the cuboid $(x, y, z) \in [0.4, 0.9] \times [0.4, 0.6] \times [0.4, 0.6]$. The computation is performed on a $(140 \times 70 \times 70)$ grid with periodic boundary conditions. The simulation time is $1\,s$.
The pressure and density fields on the outer domain boundaries at time $1\,s$ are shown in Fig. 3. We examine more precisely the pressure and density distribution along the line $y = 0.5$ in the plane $z = 0.75$ in Fig. 4. The shocks and rarefaction waves are well captured by our method, without spurious numerical oscillations. The resolution of the shocks is obviously moderate due to the coarseness of the fluid mesh.

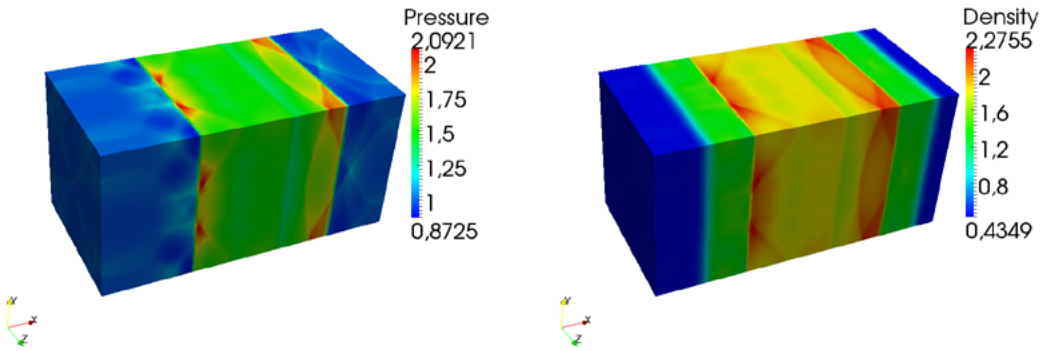

(a) (b)

Figure 3: Distribution of pressure (a) and density (b) at time $t = 1$.

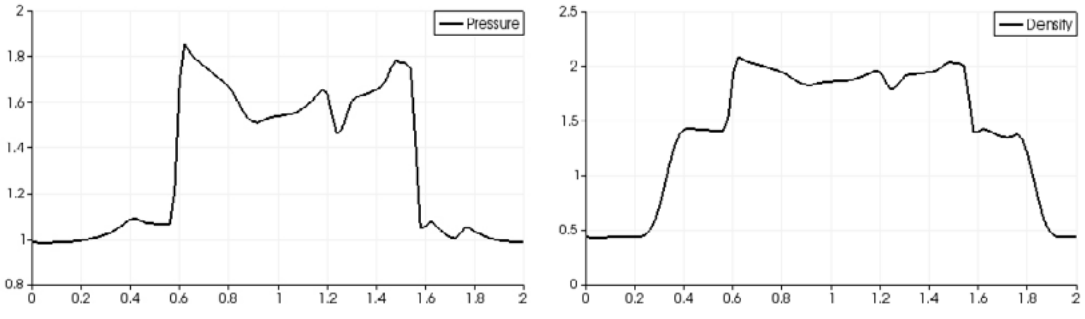

(a) (b)

Figure 4: Pressure distribution (a) and density distribution (b) along the line $y = 0.5$ in the plane $z = 0.75$ at time $t = 1$.

In Fig. 5 we present the relative conservation error of fluid mass, computed as the difference between the initial total mass value and the total mass value computed at different time steps. This mass difference

is normalized by the maximum amount of mass swept by the movement of the solid. In Fig. 6 we present the relative energy conservation error of the system, computed as the difference between the initial energy value and the energy value computed at different time steps. This energy difference is normalized by the maximum energy exchange between the fluid and solid, which is the relevant quantity to evaluate the relative effect of coupling on conservation issues.
We observe a small variation of both mass and energy, without any clear growth or decrease of either quantity. The variation of mass is as low as 0.01% of the mass swept and the variation of energy is as low as 0.4% of the energy flux in the system. We suppose that the main effect accounting for these variations are the rounding errors involved in the evaluation of geometric quantities in cut-cells, since both mass and energy are impacted at similar levels.

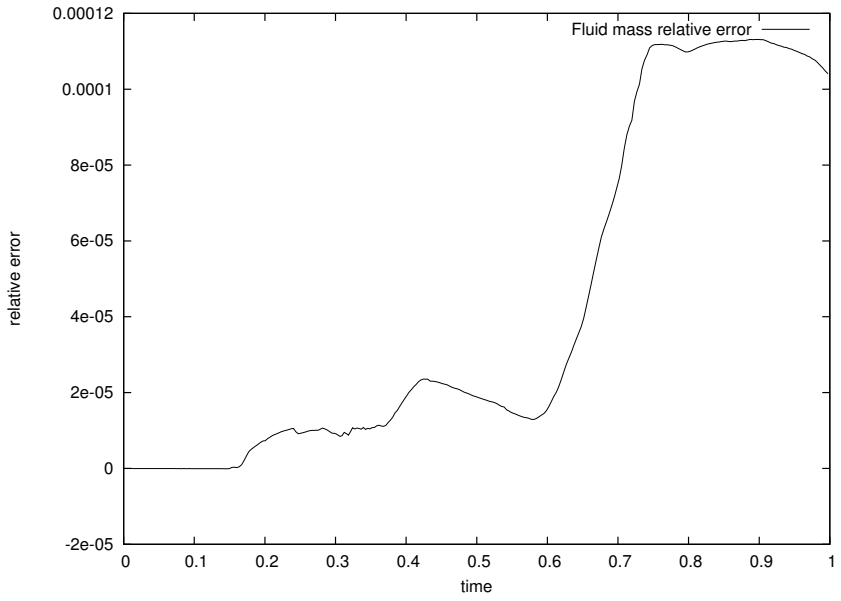

Figure 5: Relative conservation error on fluid mass.

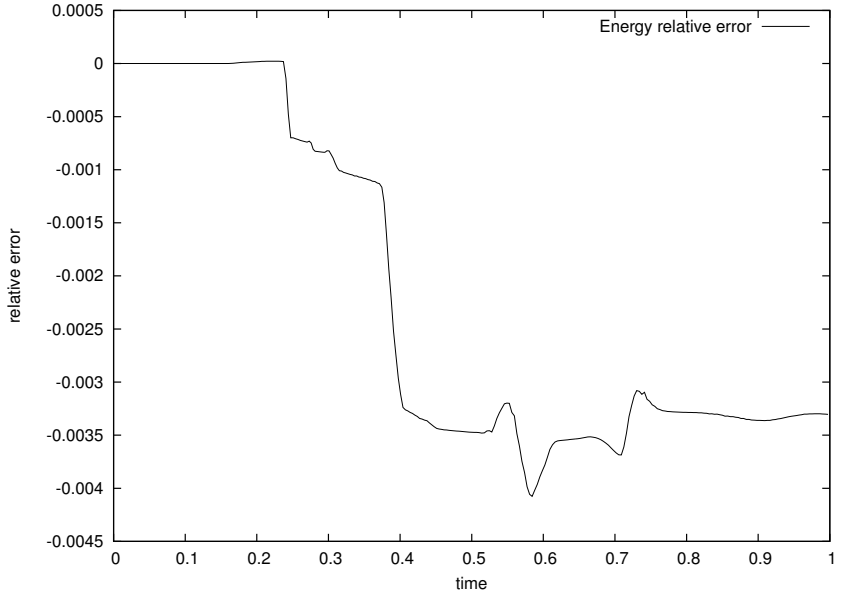

Figure 6: Relative conservation error on energy.

4.2 Interaction of a shock wave and a sphere

In this problem, a planar shock interacts with a rigid mobile sphere in a rigid channel (Fig. 7). The side boundaries of the domain are rigid walls while the left and right are respectively inflow and outflow boundaries.
The computational domain is the rectangular box $(x, y, z) \in [0, 1] \times [0, 0.2] \times [0, 0.2]$. The shock is initially set up to a Mach number of 3, so that the initial values are

$$\begin{cases} \rho = 3.857,\ p = 10.333,\ u = 2.6929,\ v = w = 0, & \text{if } x < 0.08, \\ \rho = 1,\ p = 1,\ u = v = w = 0, & \text{if } x \geq 0.08. \end{cases} \tag{12}$$

The initial position of the center of mass of the sphere is $\mathcal{C}(0.15, 0.05, 0.1)$ with radius $R = 0.05$. The sphere is approximated by a polyhedron discretized with 236 faces.
The computation is performed on a $200 \times 40 \times 40$ grid. We impose inflow and outflow boundary conditions at $x = 0$ and $x = 1$ respectively and mirror boundary conditions on the remaining outer boundaries of the fluid domain. The simulation time is $0.255s$.

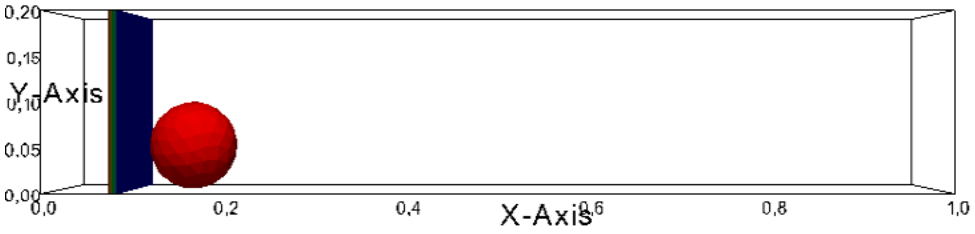

Figure 7: Initial position of the shock and sphere.

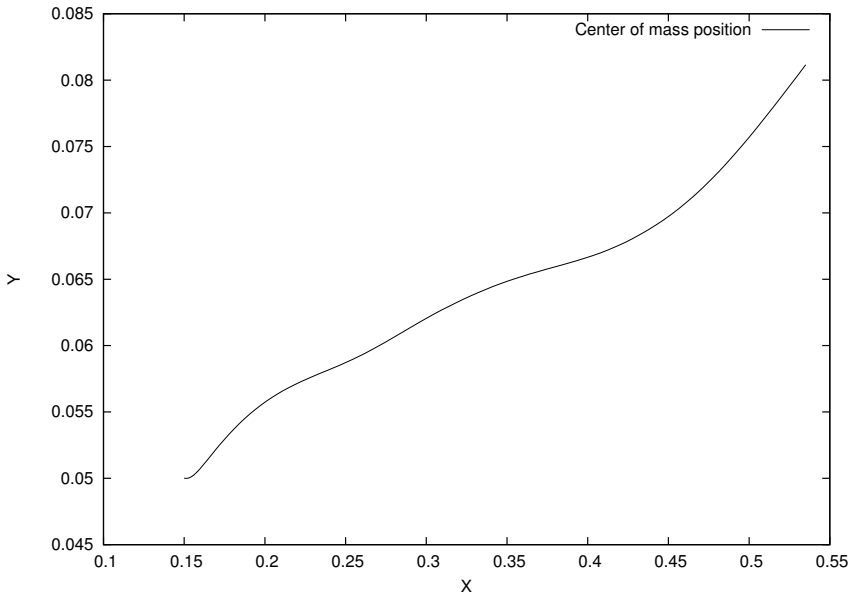

Figure 8: Trajectory of the center of mass of the sphere in the plane (x, y).

The impinging shock wave impacts the sphere and is partially reflected, while part of the shock wave moves past the sphere and part of it is transfered as kinetic energy to the sphere. The reflected shock then reflects itself on the lower wall $(y = 0)$, creating an overpressure under the sphere and lifting it up. Complex interactions between the sphere, the walls and the reflected shocks then occur. In Fig. 8 we display the trajectory of the sphere in the plane (x, y). The final position of the center of mass of the sphere is $\mathcal{C}(0.535, 0.08145, 0.0984)$. The physical system is symmetric with regard to the plane $z = 0.1$.

This feature is fairly well preserved visually by the numerical results, even though the polyhedron itself is not perfectly symmetric. As a result, the sphere mass center is no longer exactly at $z = 0.1$ at $t = 0.255$. 30 contours of density and pressure at the final time are plotted on Fig. 9a and Fig. 9b, respectively. This computation shows the ability of the coupling algorithm to compute interaction of strong discontinuities with irregular moving boundaries.

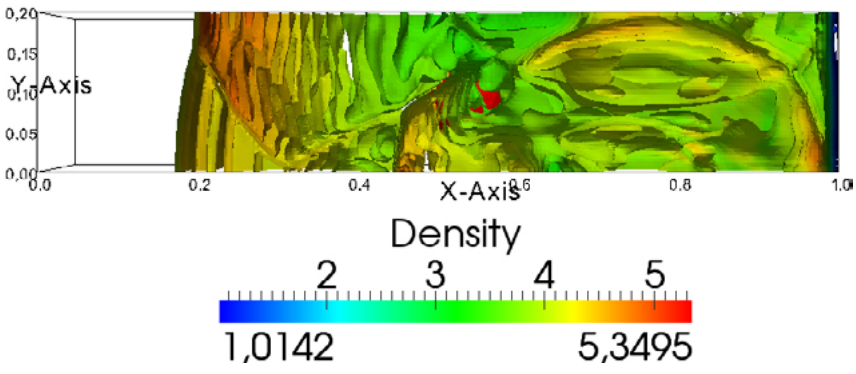

(a)

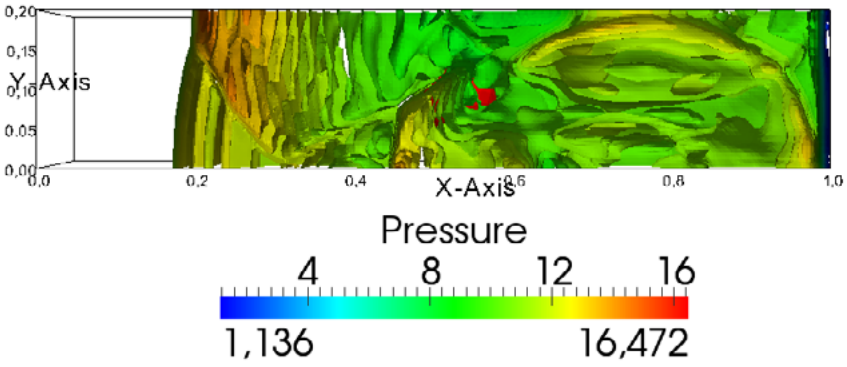

(b)

Figure 9: 30 contours of density (a) and pressure (b) at time $t = 0.255$.

REFERENCES

[1] V. Daru and C. Tenaud. High-order one-step monotonicity-preserving schemes for unsteady compressible flow calculations. *Journal of Computational Physics*, 193: 563-594, 2004.

[2] L. Monasse and C. Mariotti. An energy-preserving Discrete Element Method for elastodynamics. *ESAIM: Mathematical Modelling and Numerical Analysis*, 46: 1527-1553, 2012.

[3] L. Monasse, V. Daru, C. Mariotti, S. Piperno and C. Tenaud. A conservative coupling algorithm between a compressible flow and a rigid body using an Embedded Boundary method. *Journal of Computational Physics*, 231: 2977-2994, 2012.

[4] J. Donea, S. Guiliani and J.P. Halleux. An arbitrary lagrangian eulerian finite element method for transcient dynamics fluid structure interaction. *Computer Methods in Applied Mechanics and Engineering*, 33: 689723, 1982.

[5] C. S. Peskin Numerical analysis of blood flow in the heart. *Journal of Computational Physics*, 25: 220-252, 1977.

[6] R. P. Fedkiw. Coupling an Eulerian fluid calculation to a Lagrangian solid calculation with the Ghost Fluid method. *Journal of Computational Physics*, 175: 200-224, 2002.

[7] J. Falcovitz, G. Alfandray and G. Hanoch. A two dimensional conservation laws scheme for compressible flows with moving boundaries. *Journal of Computational Physics*, 138: 83-102, 1997.

[8] Richard B. Pember, John B. Bell, Phillip Colella, W. Y. Crutchfield and M. L. Welcome. An adaptative cartesian grid method for unsteady compressible flow in irregular regions. *Journal of Computational Physics*, 120: 278-304, 1995.

[9] X. Y. Hu, B. C. Khoo, N. A. Adams and F. L. Huang. A conservative interface method for compressible flows. *Journal of Computational Physics*, 219: 553-578, 2006.

[10] N. Favrie, S. L. Gavrilyuk and R. Saurel. Solid-fluid diffuse interface model in cases of extreme deformation. *Journal of Computational Physics*, 228: 6037-6077, 2009.

[11] S. R. Idelsohn, J. Marti, A. Limache and E. Onate. Unified Lagrangian formulation for elastic solids and incompressible fluids: Application to fluid-structure interaction problems via the PFEM. *Computer Methods in Applied Mechanics and Engineering*, 1920: 17621-1776, 2008.

[12] K. Wang, A. Rallu, J-F. Gerbeau, and C. Farhat. Algorithms for interface treatment and load computation in embedded boundary methods for fluid and fluid-structure interaction problems. *International Journal for Numerical Methods in Fluids*, 67: 1175-1206, 2011.

[13] M. A. Puscas. *Development of a numerical coupling method between a compressible fluid and a deformable structure.* PhD. thesis, University Paris-Est, France, 2014.